

Supporting Information

In-situ molecule-level interfacial tailoring of metastable intermolecular composite chip toward on-demand heat release and information encryption

*Xiaogang Guo,^{‡*a} Taotao Liang,^{‡b} Ankamfio Julius Tetteh,^a Md Labu Islam,^c Huisheng Huang,^a Binfang Yuan,^a and Xun Cui^{*d}*

^a Chongqing Key Laboratory of Inorganic Special Functional Materials, College of Chemistry and Chemical Engineering, Yangtze Normal University, Chongqing 408100, People's Republic of China

^b Chongqing Sports Medicine Center, Department of Orthopedic Surgery, Southwest Hospital, the Third Military Medical University, Chongqing 400038, People's Republic of China

^c School of Chemistry and Chemical Engineering, Beijing Institute of Technology, Beijing 102488, People's Republic of China

^d State Key Laboratory of New Textile Materials and Advanced Processing Technologies, Wuhan Textile University, Wuhan 430200, People's Republic of China

[‡] These two authors contributed equally to this work.

*Corresponding Authors. E-mail: guoxiaogang0528@126.com; xcui@wtu.edu.cn

The Supporting Information file includes:

1. Experimental Section

- 1.1 Reagents and materials
- 1.2 Construction of multifunctional MIC chip
- 1.3 Material characterization
- 1.4 Wettability analysis
- 1.5 Thermal analysis

2. Figures

Fig. S1. Theoretical output of heat of different frequently studied MIC chips, which can be divided into three levels of exothermic power of (i) top level MIC (Al/MnO₂, etc.) chips marked by light green ellipse, (ii) medium level MIC (Al/NiO, etc.) chips marked by light blue ellipse, (iii) low level MIC (Al-Ta₂O₅, etc.) chips marked by light orange ellipse.

Fig. S2. The size profile distribution of (a) fresh-SI-Al/MnO₂ MIC chip, (b) Sp-Al/MnO₂ MIC chip and (c) FSI-Al/MnO₂ MIC chip, respectively.

Fig. S3. Typical EDX spectrum analysis of (a) fresh-SI-Al/MnO₂ MIC chip, (b) Sp-Al/MnO₂ MIC chip and (c) FSI-Al/MnO₂ MIC chip, respectively.

Fig. S4. The EDX elemental distribution analysis of (a) fresh-SI-Al/MnO₂ MIC chip (b) Sp-Al/MnO₂ MIC chip and (c) FSI-Al/MnO₂ MIC chip based on the respective top-view image in **Fig. 2** (in main text).

Fig. S5. Atomic percentage of elements in fresh-SI-Al/MnO₂ MIC chip, Sp-Al/MnO₂ MIC chip and FSI-Al/MnO₂ MIC chip in three random regions.

Fig. S6. The detailed mechanism analysis of structural changes of samples with wettability-switch ability.

Fig. S7. Complete wettability switching process (a: static droplet contact state, b: completely submerged state) using three ingenious steps of (I) electro-deposition of Ag, (II) external electric field, and (III) soaking process in alcohol water, from **sample A:** fresh-SI-Al/MnO₂ MIC chip, to **sample B:** Sp-Al/MnO₂ MIC chip, to **sample C:** Sp-Al/MnO₂ MIC chip, and finally to sample B' (similar to Sp-Al/MnO₂ MIC chip) with great super-hydrophobicity, (c) the typical immersion process of

sample B and B', showing the similar mirror-like reflection phenomenon and the obvious liquid level deformation as the samples were pressed into the surface of water, and (d) the whole self-cleaning process of sample B and B' using two kinds of contaminants (oil-immersed chalk and sand powders), and the polluted surface were easily totally self-cleaned using common water droplets.

Fig. S8. Bounce process analysis of water-droplet on Sp-Al/MnO₂ MIC chip from different initial fall heights from 0.75 to 3.0 mm.

Fig. S9. (a) CA of Sp-Al/MnO₂ MIC chip after different number of wettability cycles, and (b) the wettability transition from fresh MIC chip to Sp-Al/MnO₂ MIC chip and back to FSI-Al/MnO₂ MIC chip for 5 cycles, and the relationship of CA and (c) relative humidity (RH, %) and (d) exposure time in open-air for Sp-Al/MnO₂ MIC chip.

Fig. S10. Two kinds of detail information recording and encryption processes. The relatively complex character "MIC" was conveniently marked on the MIC chip surface by constructing the hydrophobic and hydrophilic adjacent controllable interface (**STEP 1**), and then the information encryption and hiding process of the marked chip was realized by soaking in alcohol water and vacuum drying (**STEP 2**) compared with the two fully soaked MIC pictures from **STEP 1-2**. In addition, we repeated the operation of the first step to complete the information input (**STEP 3**), and realized the hydrophilic encryption of the information again by means of the additional applied electric field force (**STEP 4**). The marked characters in the enlarged area within the yellow circle are no longer visible compared with the two fully soaked MIC pictures from **STEP 3-4**.

Fig. S11. Relationship of output of heat and underwater storage time for Sp-Al/MnO₂ MIC chip and FSI-Al/MnO₂ MIC chip.

Fig. S12. Schematic drawing of the capacitor charge and discharge ignition system for the micro dual-functional MIC chip initiator, and ignition process recorded by a high-speed camera.

Fig. S13. A series of still images taken from a typical ignition deflagration study for different MIC chips, and the time interval between images is 0.1 ms.

Fig. S14. The relationship of exposure time and the output of heat of fresh Sl-Al/MnO₂ MIC chip and Sp-Al/MnO₂ MIC chip.

3. Movies

Movie S1. The wettability of fresh-Sl-Al/MnO₂ MIC chip

Movie S2. The immersion process of fresh-Sl-Al/MnO₂ MIC chip

Movie S3. The rolling-off of a water droplet on Sp-Al/MnO₂ MIC chip

Movie S4. The immersion process of Sp-Al/MnO₂ MIC chip with obvious light-reflection of soaked part

Movie S5. The wettability of FSl-Al/MnO₂ MIC chip

Movie S6. The immersion process of FSl-Al/MnO₂ MIC chip

Movie S7. The rolling-off of a water droplet on superhydrophobic MIC chip after wetting change from FSl-Al/MnO₂ MIC chip.

Movie S8. The immersion process of superhydrophobic MIC chip after wetting change from FSl-Al/MnO₂ MIC chip.

Movie S9. The first information recording process on Sp-Al/MnO₂ MIC chip, forming marked MIC chip

Movie S10. Marked MIC chip after hydrophobic encryption process

Movie S11. Second information recording process

Movie S12. Marked MIC chip after hydrophilic encryption process

4. Table

Table 1. CA of different droplets on Sp-Al/MnO₂ MIC chip surface.

1. Experimental Section

1.1 Reagents and materials

Polyethyleneimine (PEI), silver nitrate and sodium dodecyl sulfonate ($C_{12}H_{25}SO_4Na$) were supplied by Aladdin Industrial Co., China. Isopropyl alcohol (IPA) was purchased from Kelong Industrial Inc., China. Commercially available nano-Al (~60 nm, 99.9%) and manganese oxide (~100 nm, 99.9%) particles used as the high-energy fuel and oxidizer in the MICs. Other reagents (e.g. NaOH, Na_2CO_3 , tetradecane, ethanol) with analytical grade were from Sinopharm Chemical Reagent Co., China and used without further purification. The deionized water ($18M\Omega\cdot cm$) was used throughout all experiments.

1.2 Construction of multifunctional MIC chip

The multifunctional MIC chip was designed using a convenient and highly controlled technology in this study, and we selected nano-Al/MnO₂ MIC chip as a typical example. Firstly, nano-Al/MnO₂ MIC chip was fabricated by a controllable cathodic co-EPD process. Adding nano-fuel and oxidizer (mole ratio of 2.5:1) into the optimized dispersion solution of IPA and ethanol (9:1 in volume ratio) with PEI as trace additive was to form a stable suspension after sonication dispersion for 20min at room temperature. For the selection of working electrodes, after ultrasonic cleaning in ethanol and DI water repeatedly and vacuum drying at 80°C for 30min, conductive glass (ITO) and MEMS semiconductor bridge igniting components were used as two kinds of substrates for analyzing the wettability and exothermic properties, respectively, and their corresponding fixed direction and distance in suspension was vertical with 1cm and horizontal with 0.2cm in a co-EPD cell with a same free volume of 50mL. The applied field strength and deposition temperature was 20V/mm and 25°C, respectively. After co-EPD process of charged nano-fuel and oxidizer particles forced by effective electric field, the nano-Al/MnO₂ MIC films coated on working electrodes were removed into vacuum oven at 80°C for 1h. Secondly, the design of superhydrophobic nano-Al/MnO₂ MIC chip was realized by facile electrodeposition using a two-electrode setup in optimal electrolyte of silver nitrate and sodium dodecyl sulfonate (4:1 in mole ratio), where as-obtained fresh sample and

graphite-C rod were used as the anode and cathode, respectively. The distance of two electrodes and temperature was 1.0cm and 25°C, respectively, unless otherwise specified. The target superhydrophobic MIC chip was obtained after vacuum drying treatment for 10min. Thirdly, ten volts was applied to change nano-Al/MnO₂ MIC chip from super-water-repellent to superhydrophilic again for promising military application. Fourthly, the superhydrophilic chip from step III can be also changed to superhydrophobic counterpart via organic (e.g. ethanol, isopropyl alcohol) gas fumigation and vacuum drying, respectively. All samples were divided into three groups of (i) fresh superhydrophilic chip (Sl-nano-Al/MnO₂ MIC chip), (ii) superhydrophobic sample (Sp-nano-Al/MnO₂ MIC chip), and (iii) functionalized superhydrophilic sample (FSl-nano-Al/MnO₂ MIC chip).

1.3 Material characterization

The microstructures of dual functional products were studied by using an X-ray diffraction (XRD) equipment (Bruker D8 Advance, Cu K α 1) with a scanning rate of 5°/min. The surface morphology and compositions of all samples were characterized by field emission scanning electron microscope (FESEM, Tescan Mira4 operated at 15KeV) equipped with energy dispersive spectroscopy (EDS, Xplore 30), an atomic absorption spectrometer (AAS, 180-80, Exter Analytical spectrograph, USA). The chemical bonds were operated by a Fourier transform-infrared spectrometer (FT-IR, Nicolet iS10, USA) using the Attenuated Total Reflection (ATR) mode in the range of 4000 cm⁻¹-400 cm⁻¹ and a Raman spectrometer (Thermo Fisher DXR2xi, USA), respectively.

1.4 Wettability analysis

The superhydrophobic/super-hydrophilic properties of samples were investigated by an optical goniometer (SDC350, China) with a digital camera (D7000, Nikon, Japan), respectively. The wetting and water-repellent performance test was repeated five times from different random positions at room temperature, and their final average (e.g. water contact angle (CA)) was used as a virtual value. The immersion experiments were carried out in beakers and a teflon liner (Anhui Kemi Machinery Technology Co. Ltd). Different humidity environments were controlled by a salt

spray test chamber (ATEC, Co., Ltd, China), and immersion and droplet rolling tests were recorded by a high-speed camera (Phantom v7.3, Vision Research, Inc., Wayne, NJ, USA) with a Nikon AF Nikkor lens. And all samples were fixed in the perpendicular direction overwater & underwater for verifying their aging capability.

1.5 Thermal analysis

For analyzing the exothermic reaction of sample, the differential scanning calorimetry (DSC, NETZSCH, STA449F3, Germany) tests were performed under Ar (99.99999%) environment at a flow rate of 30 mL/min. All samples with ca 10mg were heated in a platinum crucible from 25°C to 1000°C at a heating rate of 30°C/min, and the corresponding heat release analysis was realized by the attached fitting software. In addition, combined with the MEMS technique, all obtained functional MIC chips based on a semiconductor bridge were ignited and detonated using the typical electric initiator equipped with a semi-automatic capacitor charge/discharge controller was applied to investigate the combustion performance of samples the ignition test of as-obtained MIC chips were investigated by an automatic capacitor charge and discharge detonator. The visual flame structure and deflagration of all MIC chips were recorded by high-speed camera (Phantom v7.3, Vision Research, Inc., Wayne, NJ, USA) at a rate of 10^4 fps.

2. Figures

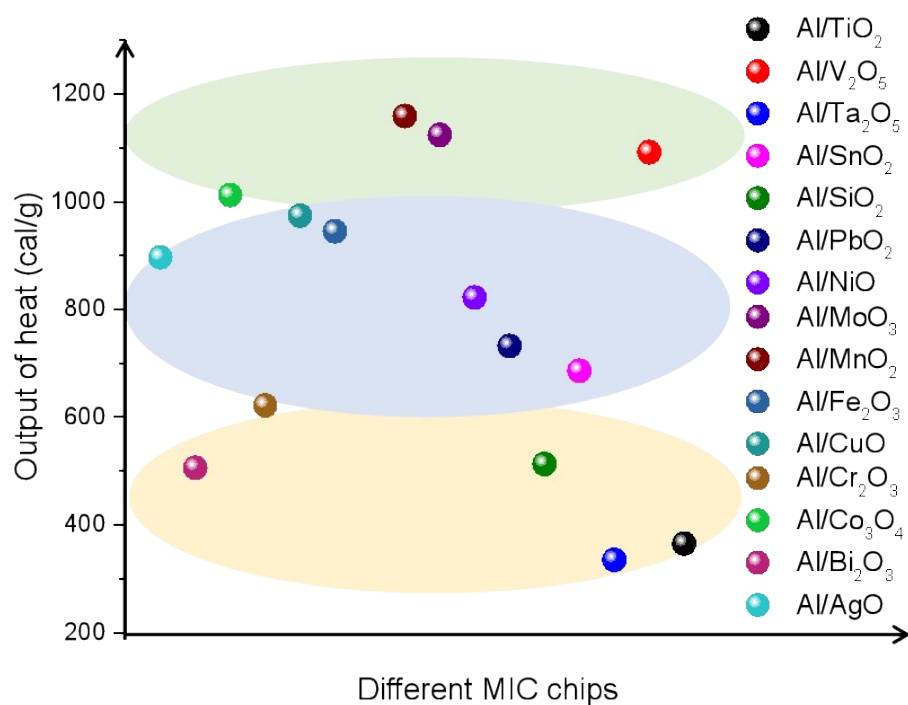


Fig. S1. Theoretical output of heat of different frequently studied MIC chips, which can be divided into three levels of exothermic power of (i) top level MIC (Al/MnO₂, etc.) chips marked by light green ellipse, (ii) medium level MIC (Al/NiO, etc.) chips marked by light blue ellipse, (iii) low level MIC (Al/Ta₂O₅, etc.) chips marked by light orange ellipse.

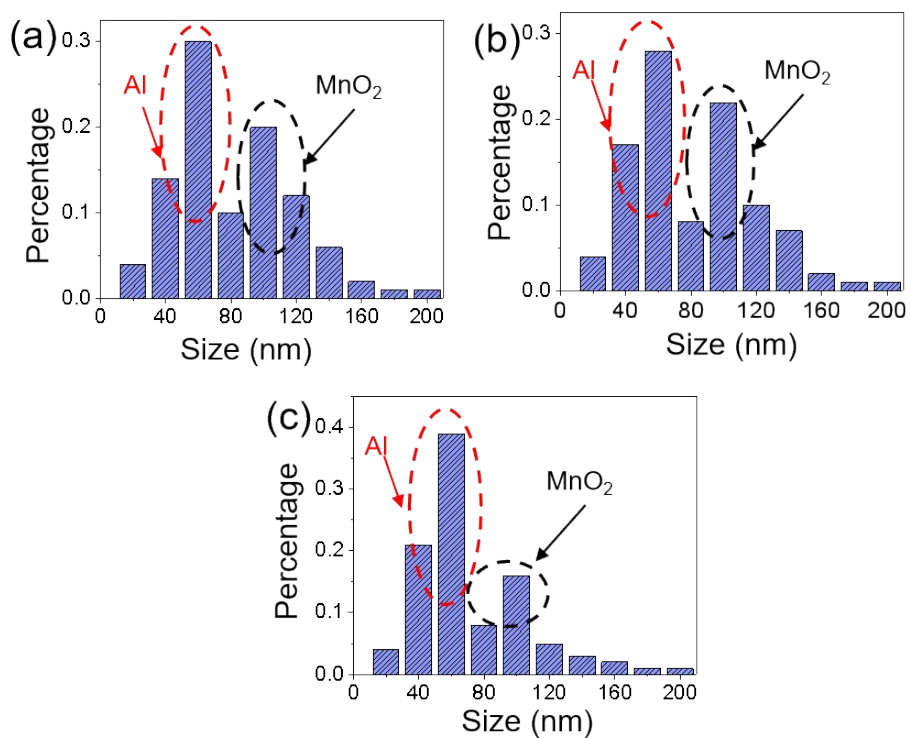


Fig. S2. The size profile distribution of (a) fresh-SI-Al/MnO₂ MIC chip, (b) Sp-Al/MnO₂ MIC chip and (c) FSI-Al/MnO₂ MIC chip, respectively.

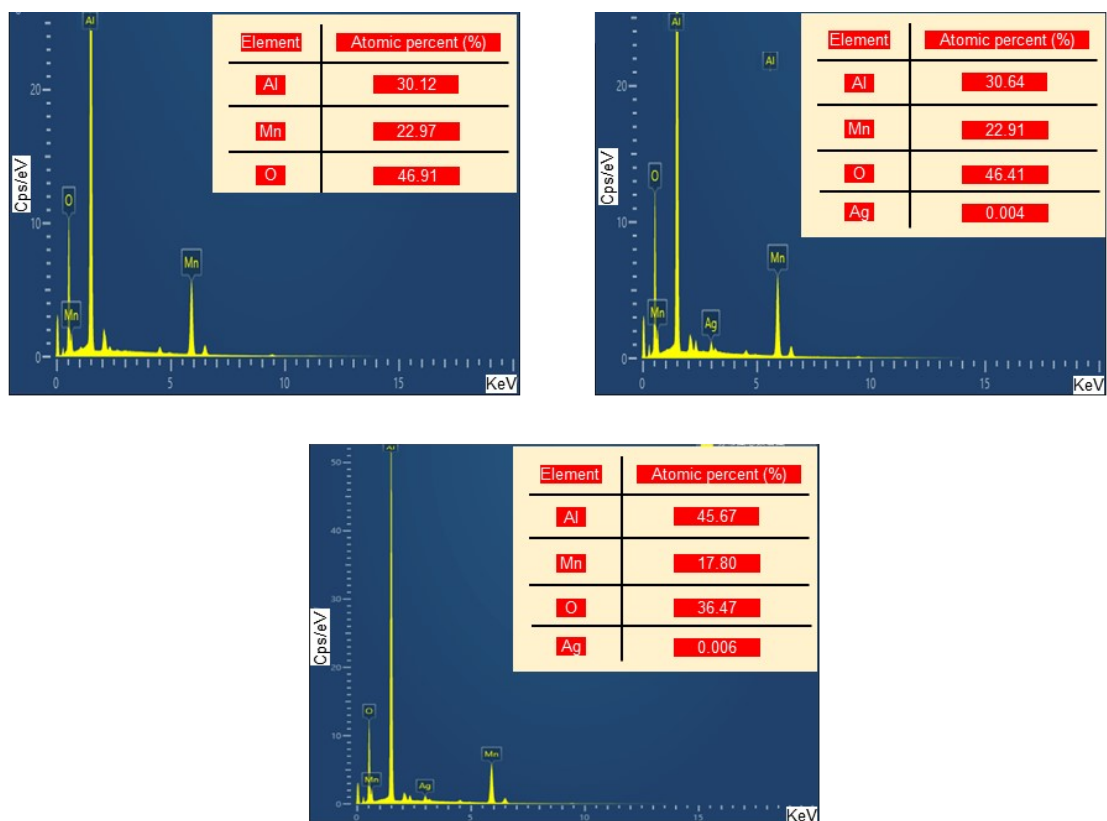


Fig. S3. Typical EDX spectrum analysis of (a) fresh-SI-Al/MnO₂ MIC chip, (b) Sp-Al/MnO₂ MIC chip and (c) FSI-Al/MnO₂ MIC chip, respectively.

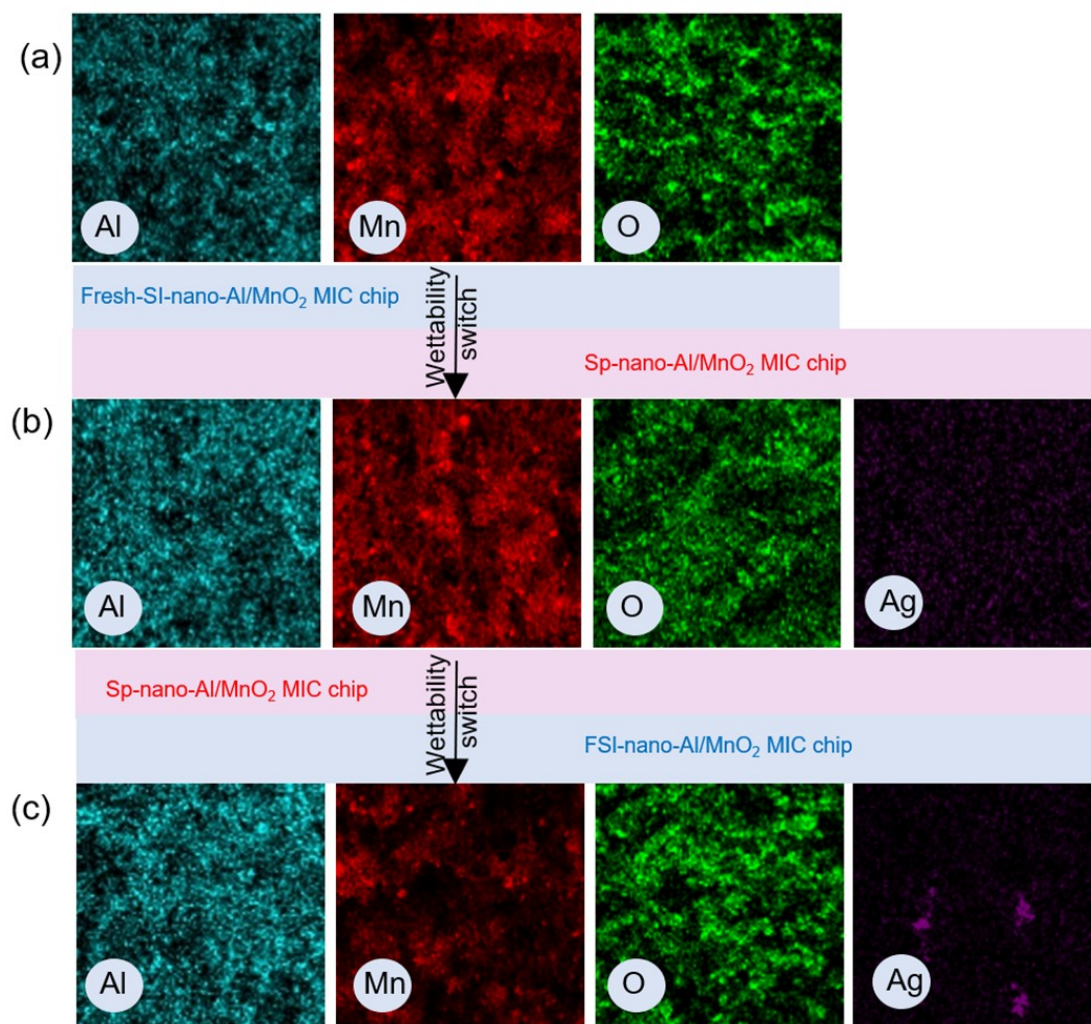


Fig. S4. The EDX elemental distribution analysis of (a) fresh-SI-Al/MnO₂ MIC chip (b) Sp-Al/MnO₂ MIC chip and (c) FSI-Al/MnO₂ MIC chip based on the respective top-view image in **Fig. 2** (in main text).

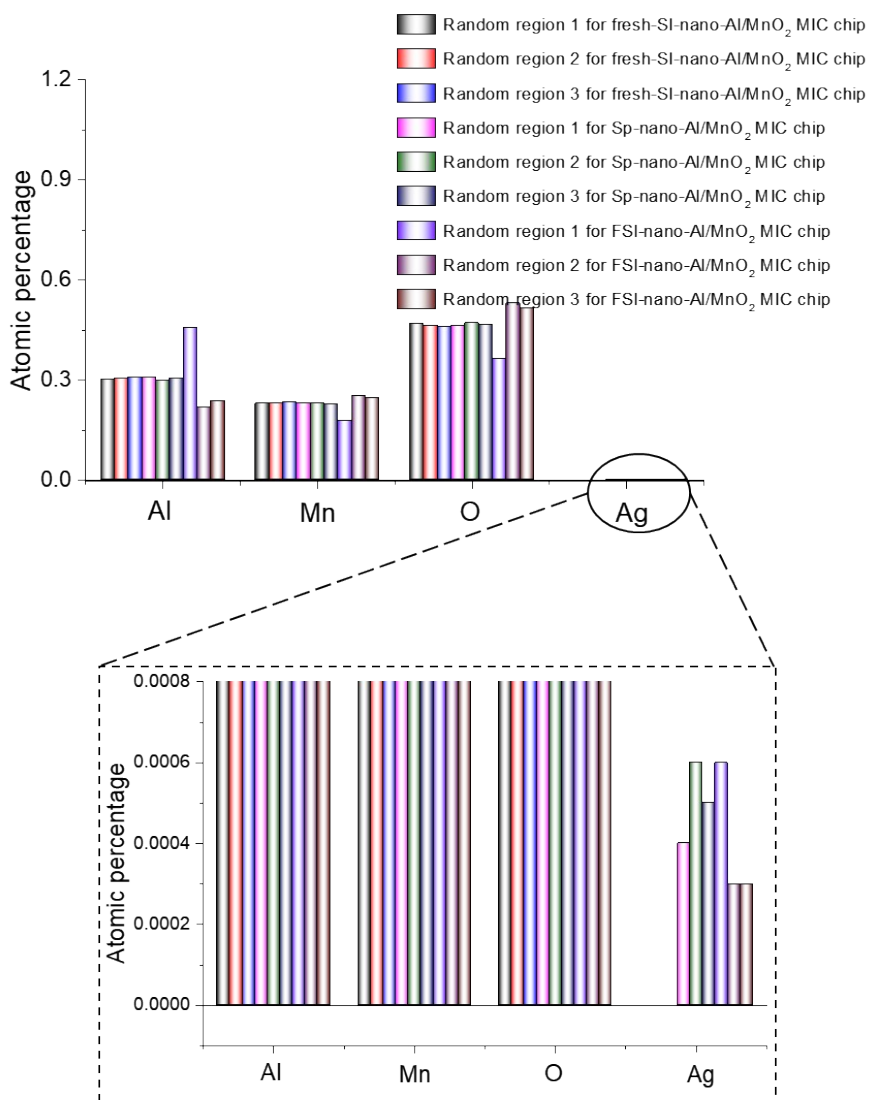


Fig. S5. Atomic percentage of elements in fresh-SI-Al/MnO₂ MIC chip, Sp-Al/MnO₂ MIC chip and FSI-Al/MnO₂ MIC chip in three random regions. For all sample, the atomic percentage of Ag is extreme small much different from that of others. The atomic percentage of main elements change a little for fresh-SI-Al/MnO₂ MIC chip, Sp-Al/MnO₂ MIC chip, but FSI-Al/MnO₂ MIC chip.

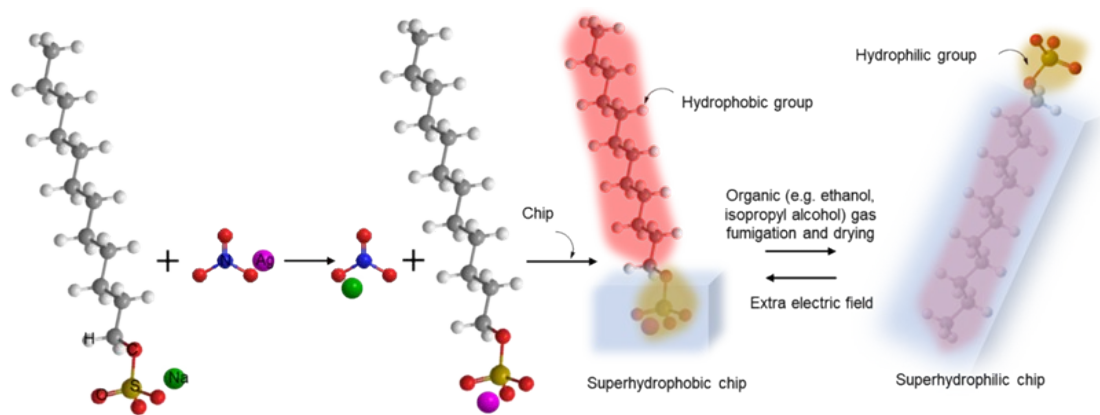


Fig. S6. The detailed mechanism analysis of structural changes of samples with wettability-switch ability.

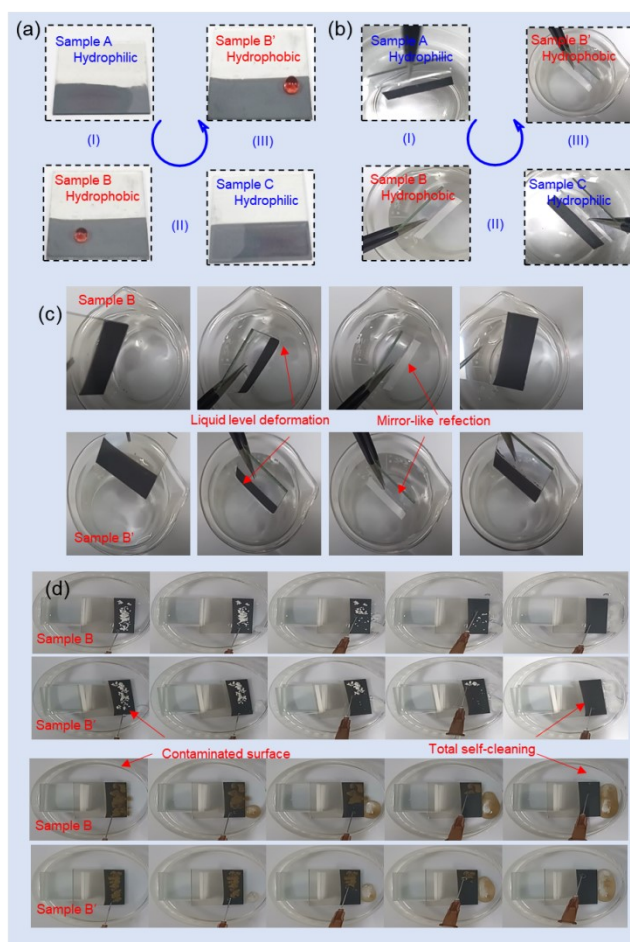


Fig. S7. Complete wettability switching process (a: static droplet contact state, b: completely submerged state) using three ingenious steps of (I) electro-deposition of Ag, (II) external electric field, and (III) soaking process in alcohol water, from **sample A:** fresh-SI-Al/MnO₂ MIC chip, to **sample B:** Sp-Al/MnO₂ MIC chip, to **sample C:** Sp-Al/MnO₂ MIC chip, and finally to sample B' (similar to Sp-Al/MnO₂ MIC chip) with great super-hydrophobicity, (c) the typical immersion process of sample B and B', showing the similar mirror-like reflection phenomenon and the obvious liquid level deformation as the samples were pressed into the surface of water, and (d) the whole self-cleaning process of sample B and B' using two kinds of contaminants (oil-immersed chalk and sand powders), and the polluted surface were easily totally self-cleaned using common water droplets.

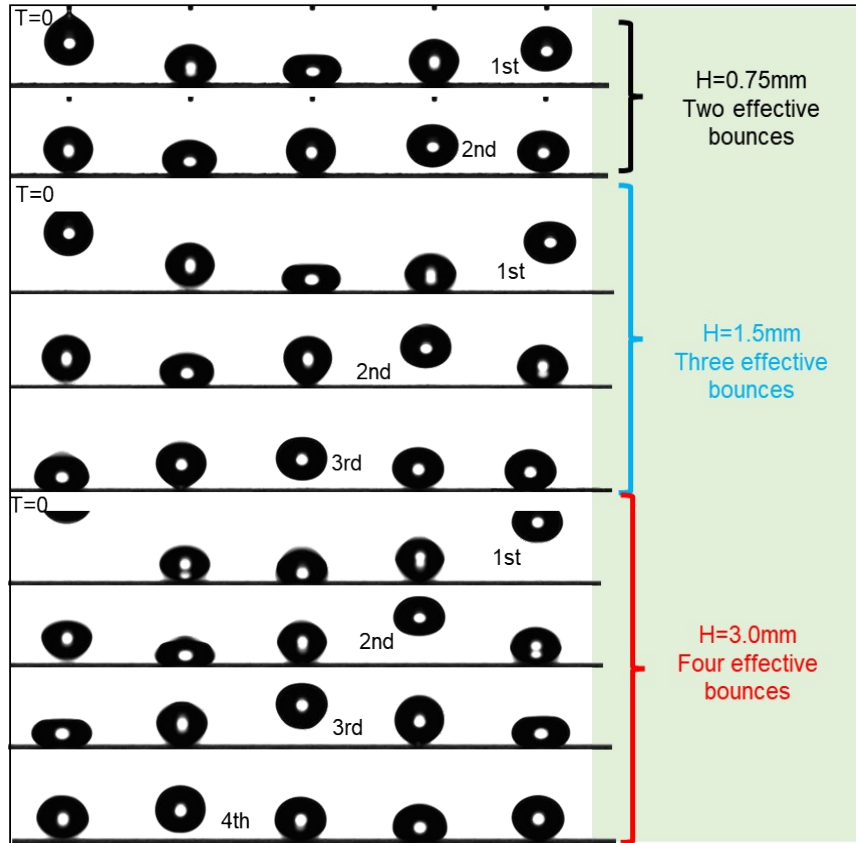


Fig. S8. Bounce process analysis of water-droplet on Sp-Al/MnO₂ MIC chip from different initial fall heights from 0.75 to 3.0 mm.

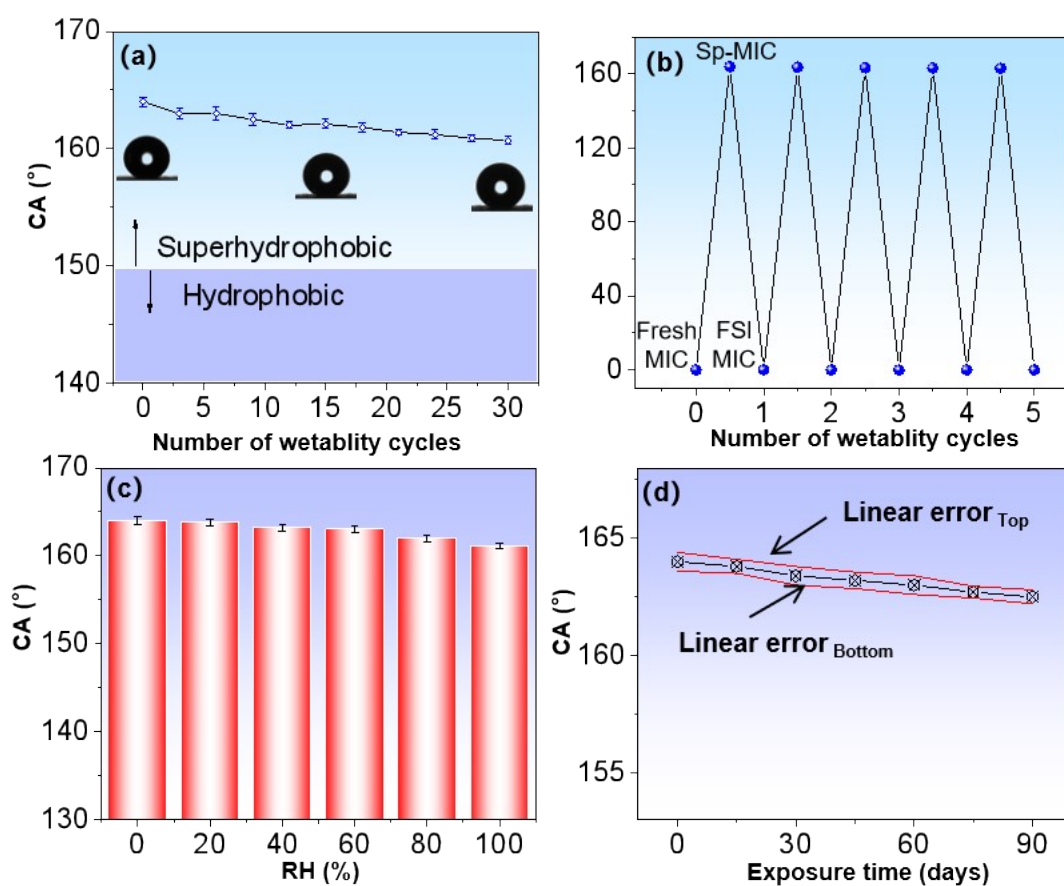


Fig. S9. (a) CA of Sp-Al/MnO₂ MIC chip after different number of wettability cycles, and (b) the wettability transition from fresh MIC chip to Sp-Al/MnO₂ MIC chip and back to FSI-Al/MnO₂ MIC chip for 5 cycles, and the relationship of CA and (c) relative humidity (RH, %) and (d) exposure time in open-air for Sp-Al/MnO₂ MIC chip.

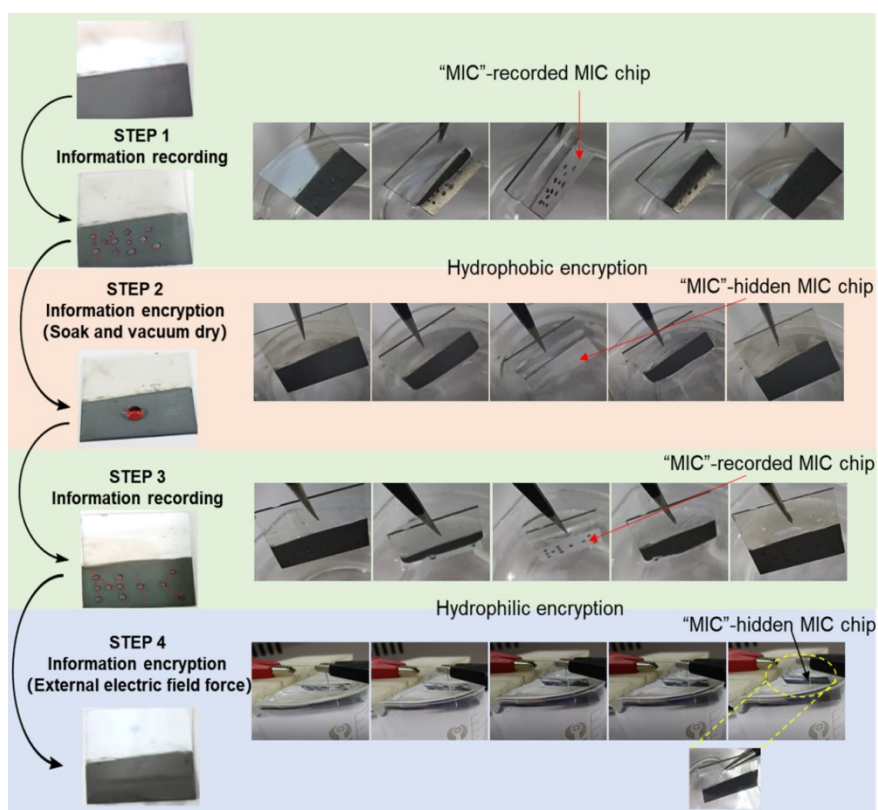


Fig. S10. Two kinds of detail information recording and encryption processes. The relatively complex character "MIC" was conveniently marked on the MIC chip surface by constructing the hydrophobic and hydrophilic adjacent controllable interface (**STEP 1**), and then the information encryption and hiding process of the marked chip was realized by soaking in alcohol water and vacuum drying (**STEP 2**) compared with the two fully soaked MIC pictures from **STEP 1-2**. In addition, we repeated the operation of the first step to complete the information input (**STEP 3**), and realized the hydrophilic encryption of the information again by means of the additional applied electric field force (**STEP 4**). The marked characters in the enlarged area within the yellow circle are no longer visible compared with the two fully soaked MIC pictures from **STEP 3-4**.

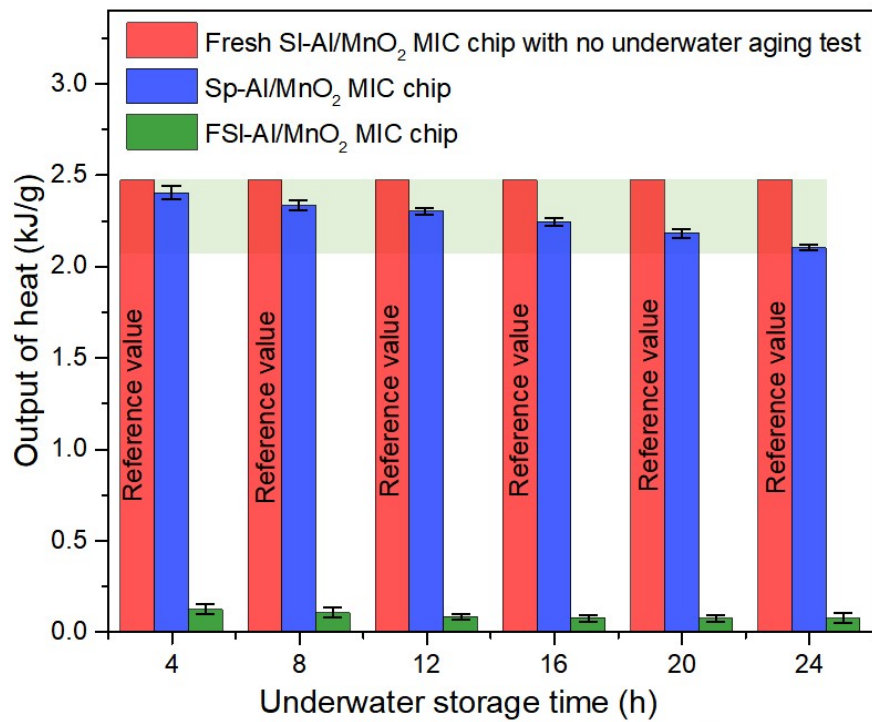


Fig. S11. Relationship of output of heat and underwater storage time for Sp-Al/MnO₂ MIC chip and FSI-Al/MnO₂ MIC chip.

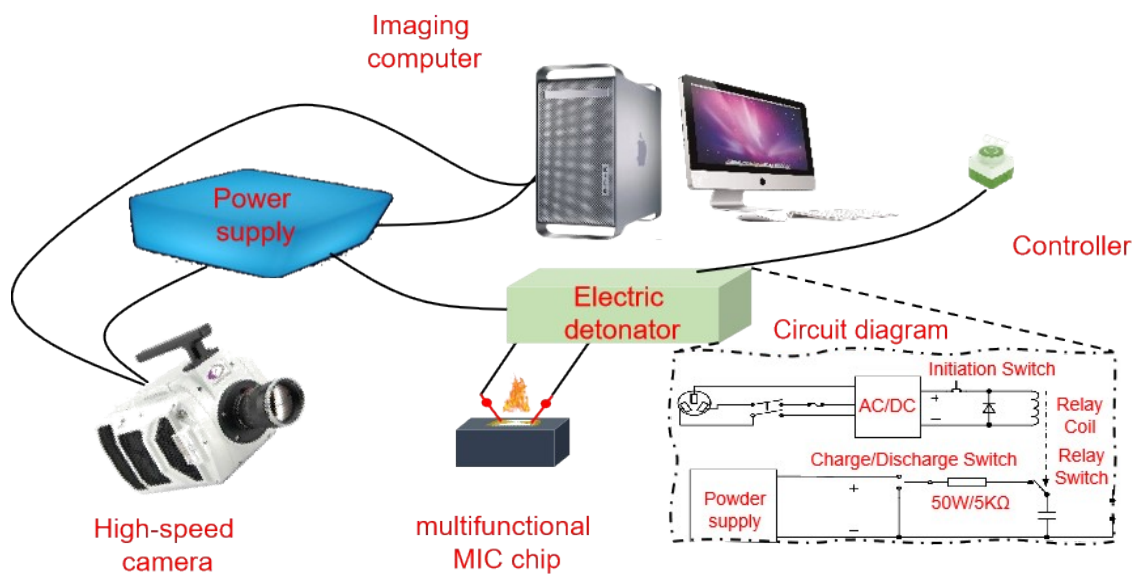


Fig. S12. Schematic drawing of the capacitor charge and discharge ignition system for the micro dual-functional MIC chip initiator, and ignition process recorded by a high-speed camera.

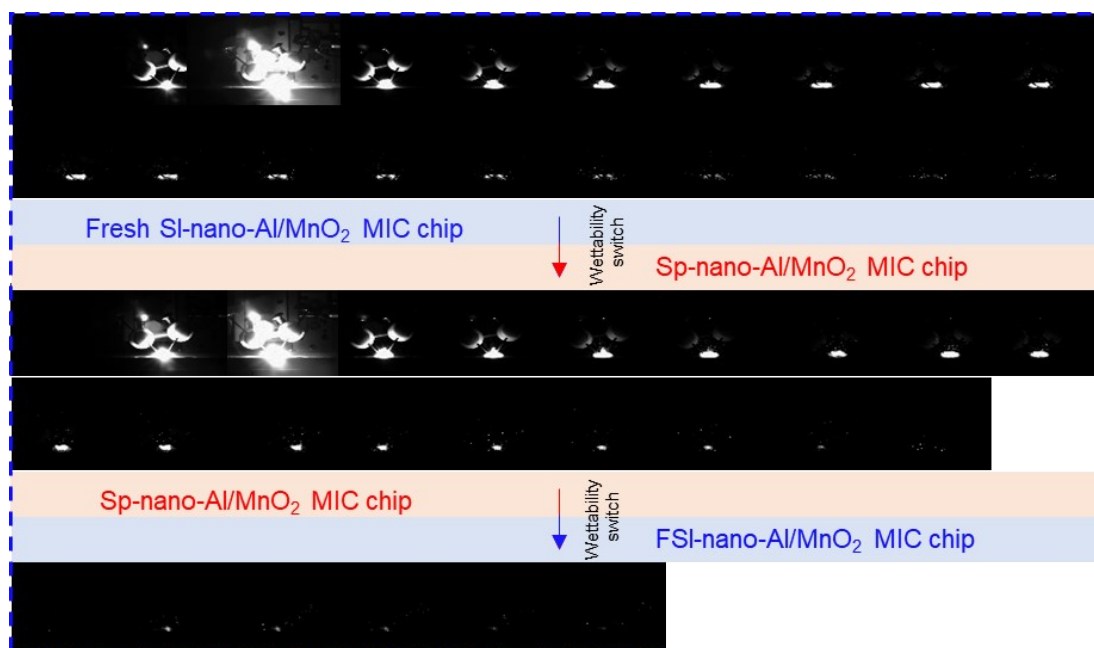


Fig. S13. A series of still images taken from a typical ignition deflagration study for different MIC chips, and the time interval between images is 0.1 ms.

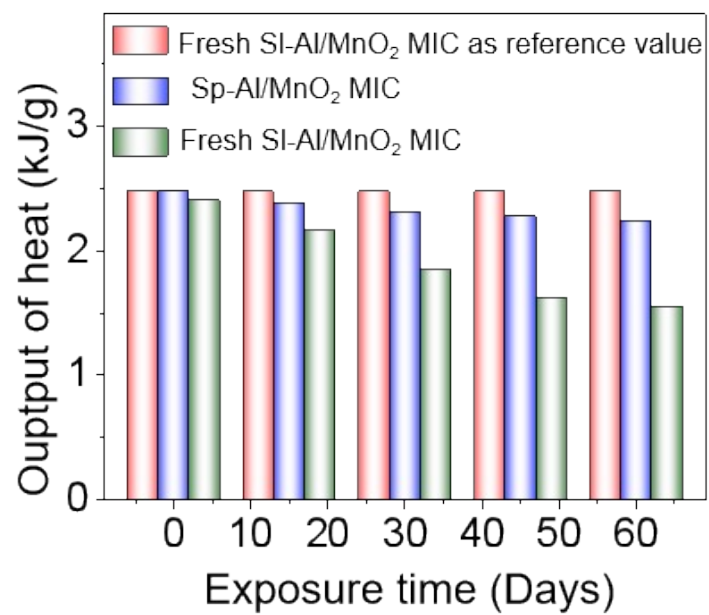


Fig. S14. The relationship of exposure time and the output of heat of fresh SI-Al/MnO₂ MIC chip and Sp-Al/MnO₂ MIC chip.

3. Movies

Movie S1. The wettability of fresh-SI-Al/MnO₂ MIC chip

Movie S2. The immersion process of fresh-SI-Al/MnO₂ MIC chip

Movie S3. The rolling-off of a water droplet on Sp-Al/MnO₂ MIC chip

Movie S4. The immersion process of Sp-Al/MnO₂ MIC chip with obvious light-reflection of soaked part

Movie S5. The wettability of FSI-Al/MnO₂ MIC chip

Movie S6. The immersion process of FSI-Al/MnO₂ MIC chip

Movie S7. The rolling-off of a water droplet on superhydrophobic MIC chip after wetting change from FSI-Al/MnO₂ MIC chip.

Movie S8. The immersion process of superhydrophobic MIC chip after wetting change from FSI-Al/MnO₂ MIC chip.

Movie S9. The first information recording process on Sp-Al/MnO₂ MIC chip, forming marked MIC chip

Movie S10. Marked MIC chip after hydrophobic encryption process

Movie S11. Second information recording process

Movie S12. Marked MIC chip after hydrophilic encryption process

4. Table

Table 1. CA of different droplets on Sp-Al/MnO₂ MIC chip surface.

Droplets	CA (°)	Error (°)
Water	164	0.6
Diiodomethane	161	0.7
Peanut oil	160	0.9
Olive oil	158	0.6
Hexadecane	156	1
Tetradecane	153	0.5